Numerical Approximation of Millimeter-Wave Frequency Sharing between Cellular Systems and Fixed Service Systems

Sungmin Han, Ji-Woong Choi, and Joongheon Kim

Abstract: **This paper presents numerical analysis and simulation results in order to study the impact of interference between fixed service (FS) systems and 5G cellular networks at 28 GHz, 38 GHz, and 60 GHz millimeter-wave (mmWave) bands. For this study, two different scenarios were considered, i.e., the aggregation of interference from small cells into an FS receiver from (i) base stations (BSs) to their associated user equipment (UE) (downlink); (ii) from UEs to their associated BSs (uplink). The simulation results determined how much interference rejection is required to protect the operation of the FS. This study is essential when using mmWave technologies in cellular networks, to determine whether the newly deployed cellular systems can co-exist with pre-deployed FS systems or not. This paper presents closed-form numerical approximation results with Taylor series approximation along with intensive simulation results. Finally, this paper confirmed that the numerical approximation results were precise, i.e., that here were only marginal differences to the intensive simulation results.**

Index Terms: **Co-Existence, fixed service systems, frequency sharing study, millimeter-wave, 5G.**

I. INTRODUCTION

ONE of the major requirements for 5G cellular systems is the achievement of multi-gigabit-per-second (multi-Gbps) rates. Millimeter-wave (mmWave) wireless technologies have primarily been considered for this application for that reasons [4]–[6], and studies have included technologies for 28 GHz [7], [8], 38/39 GHz [9], and 60 GHz [10] bands. The use of mmWave frequency bands for 5G networks provides an opportunity to use an ultra-wideband spectrum, with increased channel capacity, and the potential for spatial densification. All these benefits come at the expense of potentially greater system complexity especially in terms of radio frequency (RF) front-end and antenna design, but recent advancements in mmWave wireless systems have produced effective solutions that can be leveraged to overcome these challenges.

The other challenge in accessing mmWave bands is the protection of incumbents. In this paper, we conducted a numerical analysis as well as intensive simulations to investigate interference between mmWave cellular systems and fixed service (FS) stations at 28 GHz, 38 GHz, and 60 GHz in the same or adjacent geographical areas. Our goal was for answering to following two questions:

- How much potentially harmful interference will be injected into a FS receiver station?
- How much interference need to be suppressed to enable the co-existence of cellular networks and FS systems?

This type of numerical analysis study for calculating interference in uplink and downlink scenarios in new frequency bands is essential for discussion in ITU meetings, in order to verify whether the frequency bands are suitable for wireless network deployment or not. This type of investigation is called a *frequency sharing study* in wireless standard activities.

For this frequency sharing study, downlink and uplink interference scenarios were considered, i.e., (i) the aggregation into a fixed service receiver antenna of interference generated by every single transmission from small cell base stations to their associated mobile station (i.e., downlink interference); and (ii) the aggregation into fixed service receiver antennas of interference generated by every single transmissions from small cell mobile stations to their associated base station (i.e., uplink interference). Using 28 GHz, 38 GHz, and 60 GHz propagation characteristics and interference calculation methods, we calculated the practical amounts of frequency rejection that were necessary.

Our previous research results, which are well presented in [1]–[3], differ from the results in this paper in many ways:

- The results in [1], [2] were only a single dedicated mmWave frequency band, i.e., [1] was for 39 GHz and [2] was for 60 GHz, whereas this paper considers three major 5G candidate frequencies.
- The results in [1]–[3] only presented simulation-based results, whereas this paper illustrates numerical analysis results, and also verifies the correctness of the analysis results.
- The results in [3] presented well defined parameter setting and propagation models. However, they did not contain numerical analysis discussions which are important in terms of theoretical contributions.

Manuscript received December 29, 2019; This paper is specially handled by EICs with the help of three anonymous reviewers in a fast manner.

This work was supported by start-up funding from a Korea University grant (K1923231); by the DGIST R&D Program of the Ministry of Science and ICT(20-ST-02); and also by Institute for Information & communications Technology Promotion(IITP) grant funded by the Korea government (MSIT) (2019-0-01348).

Parts of this paper are presented in Proceedings of IEEE International Microwave Symposium (IMS), Phoenix, Arizona, May 2015 [1]; Proceedings of IEEE GLOBECOM Workshop on Millimeter-Wave Backhaul and Access: From Propagation to Prototyping (mmWave), San Diego, California, December 2015 [2]; and IEEE Access [3].

S. Han is with VSI Co., Ltd., Seoul, 05836, Republic of Korea, e-mail: shan@vsitech.co.kr.

J.-W. Choi is with Department of Information and Communication Engineering, Daegu-Gyeongbuk Institute of Science and Technology (DGIST), Daegu 771-873, Republic of Korea, e-mail: jwchoi@dgist.ac.kr.

J. Kim is with School of Electrical Engineering, Korea University, Seoul 02841, Republic of Korea, e-mail: joongheon@korea.ac.kr.

J.-W. Choi and J. Kim are corresponding authors.

Digital Object Identifier: 10.1109/JCN.2020.000001

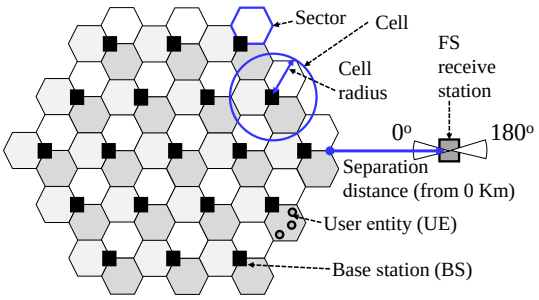

Fig. 1. Network layout [3].

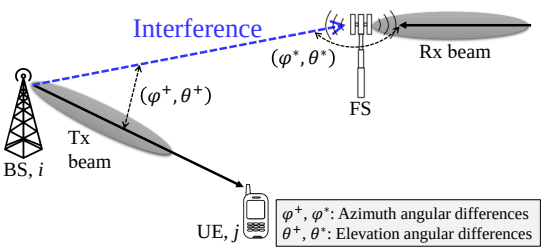

Fig. 2. Downlink interference scenarios [3].

This kind of frequency sharing study is essential before implementing mmWave technologies in cellular networks, to verify whether the newly deployed cellular systems can co-exist with the pre-deployed FS systems or not. If the frequency sharing study results indicate that both systems will generate harmful interference to each other, then the cellular network planning engineers need to implement additional functionalities to mitigate interference. On the other hand, the frequency sharing study results may indicate that no harmful interference is generated, i.e., both systems can co-exist without any additional techniques to mitigate interference. Therefore, this research is mandatory for the deployment of cellular networks of any frequency bands before deploying cellular network components.

II. MILLIMETER-WAVE FREQUENCY SHARING STUDY BETWEEN CELLULAR SYSTEMS AND FS SYSTEMS

A. Network Model for Frequency Sharing Study

The reference cellular system in this research is as Fig. 1. In this system, 19 cells are considered in a hexagonal pattern and each cell is with three sectors. Note that the cell radius is considered to be 100 m due to the short-distance ranges in mmWave wireless communication systems. Every small cell BS exists at the center of each small cell and works with a three-sector antenna. Note that the average number of active UE in each sector is assumed to be 3.

As illustrated in Fig. 1, an FS receiver station is located at the right edge of the 19 small cells at first; and here, the location point is called *origin* in this paper. In order to determine the required amount of frequency rejection, the sharing study was performed while changing the separation distances from the origin (i.e., 0 Km) up to 10 Km away the origin. Furthermore, two FS receiver antenna orientations were considered as presented in Fig. 1, i.e., 0° and 180°. The two orientations show the lower and upper bounds of system performance in terms of interference injection due to the high-directionality of mmWave radio wave propagation characteristics [1]–[3].

B. Objective and Methodologies

The objective of this study is the quantitative calculation of the amounts of *required frequency rejection* as the function of separation distances which can allow the compatible operation of FS systems and mmWave cellular systems. For this frequency sharing study, two separated interference scenarios (i.e., downlink vs. uplink) were considered, as mentioned before.

After calculating the accumulated interferences in the two downlink and uplink interference scenarios, the required frequency rejection should satisfy the protection requirements of the FS receiver antenna (denoted as R) can be calculated as follows, in order to guarantee the co-existence without interference mitigation schemes:

$$R = \mathcal{I} - \mathcal{N} - \gamma_{\text{requirement}}, \tag{1}$$

where $\mathcal{I}$ is the accumulated co-channel and adjacent-channel interference; $\mathcal{N}$ means the FS receiver antenna noise power as

$$\mathcal{N} = N_{\text{FS}}^{\text{thermal}} + 10\log_{10}\left(\frac{B_{\text{FS}}}{10^6}\right) + N_{\text{FS}}^{\text{F}}, \tag{2}$$

where $N_{\text{FS}}^{\text{thermal}}$ is an FS receiver thermal noise [11], B_{FS} is an FS channel bandwidth, N_{FS}^{F} is an FS receiver noise figure [11], and $\gamma_{\text{requirement}}$ in (1) means the required interference-per-noise for FS operation protection (set to -10 dB).

In this decision criteria,

- If $\mathcal{I}^*$ is smaller than $\gamma_{\text{requirement}}$, any kinds of interference injection suppression schemes are not required according to the fact that the co-existence of FS systems and cellular systems is possible without interference rejection.
- If $\mathcal{I}^*$ is larger than $\gamma_{\text{requirement}}$, $\mathcal{I}^* - \gamma_{\text{requirement}}$ amounts of interference should be suppressed in order to to enable the co-existence of FS systems and cellular systems.

C. Downlink Co-Channel Interference

In order to calculate a single downlink interference component, $I_{(i,j)}^{\text{DL}}$, i.e., an interference to an FS receiver generated by the wireless transmission from a cellular BS i to its UE j,

$$\begin{aligned} I_{(i,j)}^{\text{DL}} = {} & f_{\text{BW-scale}}\left(P_{\text{BS},i} + G_{\text{BS},i}^{\text{Tx}}\left(\varphi^+, \theta^+\right)\right) \\ & - L\left(f_c, d_i\right) + G_{\text{FS}}^{\text{Rx}}\left(\varphi^*, \theta^*\right), \end{aligned} \tag{3}$$

where the function $f_{\text{BW-scale}}(\cdot)$ is defined as

$$f_{\text{BW-scale}}\left(x\right) = 10\log_{10}\left(\frac{B_{\text{FS}}}{B_{\text{BS}}} \times 10^{(x/10)}\right), \tag{4}$$

should be calculated where $I_{(i,j)}^{\text{DL}}$ is the interference to the FS receive antenna due to the downlink wireless transmission from small-cell BS i to its UE j, $G_{\text{BS},i}^{\text{Tx}}\left(\varphi^+, \theta^+\right)$ means the transmit antenna gain to the FS receiver antenna by the downlink wireless transmission from the cellular BS i to its UEs; and the angular differences between the downlink wireless transmission and interference directions in the azimuth and elevation planes are

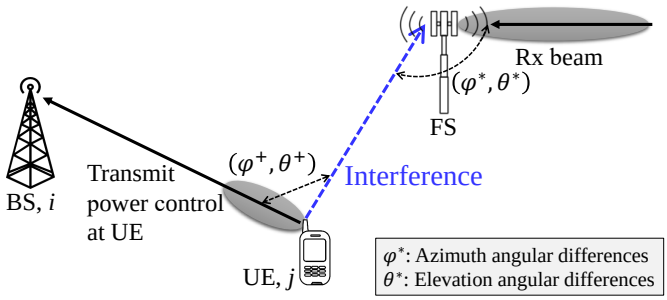

Fig. 3. Uplink interference scenarios [3].

denoted as φ^+ and θ^+ and are presented in Fig. 2. For the angular difference calculation, the FS, BS, and UE heights are 30 m, 6 m, and 1.5 m, respectively. In addition, it should consider that certain portion of the transmit power from BS i affects an FS receiver antenna according to the fact that the bandwidths in the BS and FS are not same to each other. Therfore, it is obvious that the received interference at an FS receive antenna is proportional to the bandwidth difference, i.e., the received power at an FS receiver from a cellular BS i (i.e., $f_{\text{BW-scale}}(x)$) can be as (4) by [3] where B_{FS} and B_{BS} are the bandwidths in an FS system and a small-cell BS (set to 200 MHz in the 28 GHz band, 500 MHz in the 38 GHz band, and 2.16 GHz in the 60 GHz band), respectively. Note that the bandwidth in BS is same as that of UE. Moreover, $G_{\text{FS}}^{\text{Rx}}(\varphi^*, \theta^*)$ in (3) is the FS receive antenna gain by the downlink wireless transmission from the cellular BS i to its UE and the corresponding angular differences in azimuth and elevation planes (i.e., φ^* and θ^*) is calculated as presented in Fig. 2. In order to calculate $G_{\text{BS},i}^{\text{Tx}}(\varphi^+, \theta^+)$ and $G_{\text{FS}}^{\text{Rx}}(\varphi^*, \theta^*)$, the ITU-recommended reference antenna radiation patterns are needed for BS and FS; the details about the reference radiation patterns are in Appendix. In (3), $L(f_c, d_i)$ means the mmWave wireless signal path-loss attenuation from cellular BS i to FS receive antenna; where it can be calculated as follows:

$$L(f_c, d_i) = PL(f_c, d_i) + O(f_c, d_i) + R(f_c, d_i), \quad (5)$$

where $PL(f_c, d_i)$, $O(f_c, d_i)$, and $R(f_c, d_i)$ are path-loss (calculated with (20)), attenuation due to oxygen absorption (0.11 dB/Km, 0.13 dB/Km, and 16 dB/Km at 28 GHz, 38 GHz, and 60 GHz as presented in Appendix), and rain attenuation (refer to Table 2 in Appendix). When every single downlink interference with (3) is calculated, the overall accumulated interference (i.e., $\mathcal{I}$ in (1)) in an FS receiver antenna can be computed by the summation of the individual downlink interference values in a linear scale:

$$\mathcal{I} = \sum_{\forall i \in S_{\text{BS}}} \sum_{\forall j \in S_{\text{UE},i}} I_{(i,j)}^{\text{DL}}, \quad (6)$$

where S_{BS} is a set of cellular BSs and $S_{\text{UE},i}$ is the set of UEs that is associated with cellular BS $i \in S_{\text{BS}}$.

D. Uplink Co-Channel Interference

In order to calculate a single uplink interference component, $I_{(j,i)}^{\text{UL}}$, i.e., an interference to an FS receive antenna by the wireless transmission from UE j to its BS i,

$$I_{(j,i)}^{\text{UL}} = f_{\text{BW-scale}}\left(P_{\text{UE},j}^{\text{Tx}} + G_{\text{UE},j}^{\text{Tx}}(\varphi^+, \theta^+)\right) - L(f_c, d_j) + G_{\text{FS}}^{\text{Rx}}(\varphi^*, \theta^*) \quad (7)$$

is calculated where $I_{(j,i)}^{\text{UL}}$ is the interference to the FS receiver antenna by the wireless transmission from UE j to its cellular BS i, and $P_{\text{UE},j}^{\text{Tx}}$ is UE transmit power at UE j. Here, LTE-like uplink power control is considered, i.e., the transmit power at UE is controlled as follows [12]:

$$P_{\text{UE},j}^{\text{Tx}} = P_{\max} \times \min\left\{1, \max\left[R_{\min}, \left(\frac{PL}{PL_{x-ile}}\right)^{\gamma}\right]\right\}, \quad (8)$$

where $P_{\text{UE},j}^{\text{Tx}}$ stands for the transmit power at UE j. More details about this TPC at UE for frequency sharing study are presented and summarized in [2], [3]. Here, $L(f_c, d_j)$ and $G_{\text{FS}}^{\text{Rx}}(\varphi^*, \theta^*)$ are explained in Section II.C; and the related illustrations are shown in Fig. 3. Moreover, the bandwidth difference between FS and UE is also considered via (4).

When every single uplink interference with (7) is calculated, the overall accumulated uplink interference (i.e., $\mathcal{I}$ in (1)) in an FS receiver antenna can be computed by the summation of all uplink interference components in a linear scale:

$$\mathcal{I} = \sum_{\forall i \in S_{\text{BS}}} \sum_{\forall j \in S_{\text{UE},i}} I_{(i,j)}^{\text{UL}}, \quad (9)$$

where S_{BS} stands for the set of cellular BSs and $S_{\text{UE},i}$ means the set of the UEs which are associated with the cellular BS $i \in S_{\text{BS}}$.

E. Adjacent-Channel Interference Calculation

Besides the co-channel interference components which can be calculated by the methodologies in Section II.C and Section II.D, the interference components by adjacent channel sensitivity should be considered because the bandwidth of BS/UE is much larger than the one of FS. In this paper, 40 dB, 50 dB, and 60 dB less interference values are used compared to the co-channel interference values in the first, second, and third adjacent channel interference, respectively.

The $\mathcal{I}^*$ in (1) can be compute by the summation (in a linear scale) of co-channel interference $\mathcal{I}$ ((6) for downlink and (9) for uplink) and adjacent channel interference.

III. SIMULATION RESULT INTERPRETATION

The simulation results can be generally illustrated as shown in Fig. 4. In Fig. 4, x-axis and y-axis are the distance between the 19 cells and the FS receiver and the required frequency rejection R, respectively; and then R can be obtained by (1). If R in Fig. 4 is positive, R amount of interference should be suppressed, and thus interference mitigation schemes should be introduced for operating the FS receiver antenna without any harmful interference impacts. On the other hand, when the R equals to zero or less than zero, interference suppression is not required.

The plotting results in Fig. 4 show different behaviors depending on the separation distance, i.e., generally, the regions [A], [B], and [C]. For explaining the behaviors, we have a sample

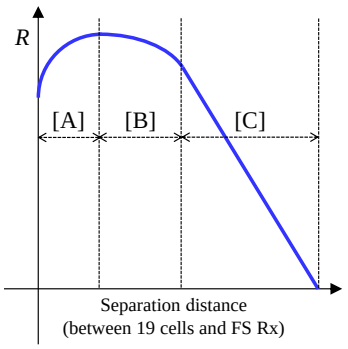

Fig. 4. Simulation result interpretation [3].

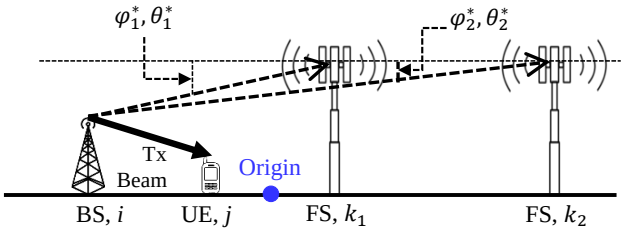

Fig. 5. Illustration for interpreting the graph in [A] and [B] in Fig. 4. Note that the *origin* in this figure means the point where the separation distance is 0 Km (refer to Section II.A).

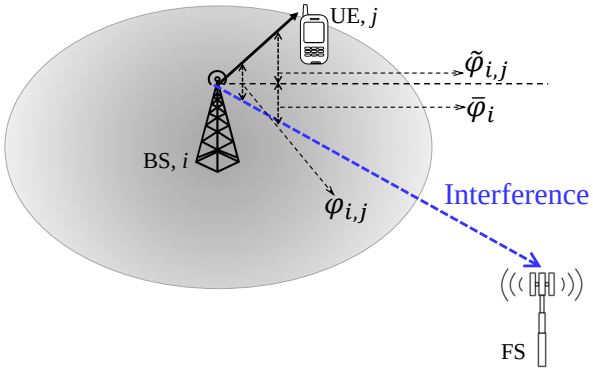

Fig. 6. Top view of co-channel downlink interference model geometry (azimuth).

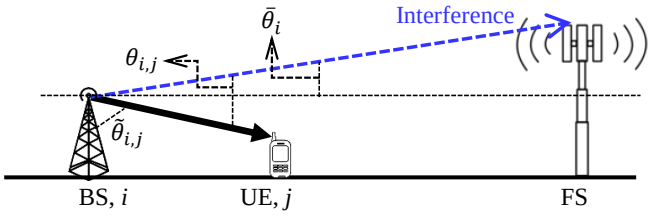

Fig. 7. Side view of co-channel downlink interference model geometry (elevation).

geometry in Fig. 5. In Fig. 5, two R values are compared when the FS Rx antennas are at k_1 or k_2 positions. In [A], the distance between the origin and k_1 is small, and the distance between the origin and k_2 is also small; and finally, k_1 is closer to the origin than k_2. In this case, θ_1^* and θ_2^* can be defined as presented in Fig. 5 and Section II.C, Section II.D, Fig. 2, and Fig. 3. Then,

$$G_{\mathrm{FS}}^{\mathrm{Rx}}\left(\varphi_1^*, \theta_1^*\right) < G_{\mathrm{FS}}^{\mathrm{Rx}}\left(\varphi_2^*, \theta_2^*\right), \tag{10}$$

when k_2 is farther from origin than k_1. Moreover, $L\left(f_c, d_i\right)$ (in (5), i.e., path-loss including oxygen/rain attenuation) is not yet dominant if the distance between BS i and FS Rx is small. Therefore, it is obvious the R increases as the FS receiver station becomes farther from the origin within region [A]. In [B], the impacts of $L\left(f_c, d_i\right)$ (in (5) increase when the separation distance becomes longer. Moreover, the angular difference between θ_1^* and θ_2^* becomes smaller. Thus, the R starts to decrease. In [C], the R linearly decreases in a dB scale according to the fact that the impacts from $L\left(f_c, d_i\right)$ become much larger than the impacts in [B].

IV. CLOSED-FORM APPROXIMATED NUMERICAL ANALYSIS

In this section, we discuss the non-linearity in the dB scale of R. Since R is obtained as (1), the analysis of interference can reflect the characteristics of R. In the interference analysis, a simplified co-channel downlink interference model is used as follows:

$$\mathcal{I}^* = \sum_i \sum_j \beta_a(\varphi_{i,j})\beta_e(\theta_{i,j}) d_i^n, \tag{11}$$

where d_i is the distance between the ith BS and the FS receiver station, n is a pathloss exponent, and $\beta_a(\varphi_{i,j})$, $\beta_e(\theta_{i,j})$ are the azimuth and elevation antenna gains from the ith BS to the FS receiver when the ith BS tends to transmit to its jth UE, respectively. $\varphi_{i,j}$ and $\theta_{i,j}$ are the angles of the FS, ith BS and jth BS of the ith BS in the azimuth and elevation planes as shown in Figs. 6 and 7, respectively. The $\varphi_{i,j}$ and $\theta_{i,j}$ can be expressed as $\varphi_{i,j} = \tilde{\varphi}_{i,j} - \bar{\varphi}_i$ and $\theta_{i,j} = 0.5\pi + \bar{\theta}_i - \tilde{\theta}_{i,j}$. Note that the $\bar{\theta}_i$ and $\bar{\varphi}_i$ are only dependent on the locations of BSs and FS (i.e., they are independent of the locations of the UEs).

When the FS and BSs are fixed and the UEs are random, the expectation of (11), i.e., $E_{\tilde{\varphi},\tilde{\theta}}\left[\mathcal{I}^*\right]$, can be expressed as follows:

$$\begin{aligned}
E_{\tilde{\varphi},\tilde{\theta}}\left[\mathcal{I}^*\right] &= E_{\tilde{\varphi},\tilde{\theta}}\left[\sum_i \sum_j \beta_a(\varphi_{i,j})\beta_e(\theta_{i,j}) d_i^n\right] \\
&= E_{\tilde{\varphi},\tilde{\theta}}\left[\sum_i \sum_j \beta_a(0.5\pi + \bar{\varphi}_i - \tilde{\varphi}_{i,j})\beta_e(\tilde{\theta}_{i,j} - \bar{\theta}_i) d_i^n\right] \\
&= \sum_i \sum_j E_{\tilde{\varphi}}\left[\beta_a(0.5\pi + \bar{\varphi}_i - \tilde{\varphi}_{i,j})\right] E_{\tilde{\theta}}\left[\beta_e(\tilde{\theta}_{i,j} - \bar{\theta}_i)\right] d_i^n \\
&= N_{\mathrm{UE}} \sum_i E_{\tilde{\varphi}}\left[\beta_a(0.5\pi + \bar{\varphi}_i - \tilde{\varphi}_{i,j})\right] E_{\tilde{\theta}}\left[\beta_e(\tilde{\theta}_{i,j} - \bar{\theta}_i)\right] d_i^n,
\end{aligned} \tag{12}$$

where N_{UE} is the number of UEs per BS.

The probability density functions (PDFs) of $\tilde{\varphi}$ and $\tilde{\theta}$ are determined by the distribution of the UEs. If the UEs are uniformly distributed in given cell area whose radius is ρ, the PDFs of $\tilde{\varphi}$

Table 1. Parameters and models in various mmWave bands [3].

		28 GHz	38 GHz	60 GHz
FS parameters	Rx antenna gain at FS k: $G^{\text{Rx}}_{\text{FS},k}(0,0)$			39.2 dBi
	Height: h_{FS} [13]			30 m
	Channel bandwidth: B_{FS} [11]	60 MHz	56 MHz	50 MHz
	Rx noise figure: N^{F}_{FS} [11]	8 dB	6.3 dB	7 dB
	Thermal noise at Rx: $N^{\text{thermal}}_{\text{FS}}$ [11]	-136 dBm/Hz	-137.7 dBm/Hz	-137 dBm/Hz
	Required I/N for protection of FS: $\gamma_{\text{requirement}}$ [11]			-10 dB
BS parameters	The number of deployed BSs			19
	The number of sectors in each BS cell			3
	Cell radius r			100 m
	Tx antenna gain at BS i: $G^{\text{Tx}}_{\text{BS},i}(0,0)$	18.0 dBi	20.1 dBi	24 dBi
	Tx power at BS i: $P_{\text{BS},i}$	11.4 dBm	14.0 dBm	19 dBm
	Height: h_{BS} [14]			6 m
	Channel bandwidth: B_{BS}	200 MHz	500 MHz [1]	2.16 GHz [14]
UE parameters	The number of active UEs in each sector			3
	Tx antenna gain	9.0 dBi	11.1 dBi	15 dBi
	Maximum Tx power at UE j: $P^{\max}_{\text{UE},j}$	2.4 dBm	5 dBm	10 dBm
	Minimum Tx power at UE j: $P^{\min}_{\text{UE},j}$	-47.6 dBm	-45 dBm	-40 dBm
	Height: h_{UE} [14]			1.5 m
	Channel bandwidth: B_{UE}	200 MHz	500 MHz [1]	2.16 GHz [14]

and $\tilde{\theta}$ are as follows:

$$f_{\tilde{\Phi}}(\tilde{\varphi}) = \frac{1}{2\pi},\ \pi < \tilde{\varphi} \leq \pi$$

$$f_{\tilde{\Theta}}(\tilde{\theta}) = 2\left(\frac{H}{\rho}\right)^2 \tan(\tilde{\theta})\sec^2(\tilde{\theta}),\ 0 < \tilde{\theta} \leq \tan^{-1}\left(\frac{\rho}{H}\right),$$

where $f_{\tilde{\Phi}}(\tilde{\varphi})$ and $f_{\tilde{\Theta}}(\tilde{\theta})$ are the PDFs of $\tilde{\varphi}$ and $\tilde{\theta}$, respectively, and H is the height of the BS. Although the integration of $\beta_e(\cdot)$ can be expressed in a closed form, computing $E_{\tilde{\theta}}[\beta_e(\tilde{\theta}_{i,j} - \bar{\theta}_i)]$ in a closed form is difficult because $f_{\tilde{\Theta}}(\tilde{\theta})$ is a trigonometric function. However, since in most cases $\tilde{\theta}$ is a value near 0, $f_{\tilde{\Theta}}(\tilde{\theta})$ can be approximated without a critical error, and an approximation using the Taylor series is helpful for computing the closed form. The approximation of $f_{\tilde{\Theta}}(\tilde{\theta})$ is

$$f_{\tilde{\Theta}}(\tilde{\theta}) \approx 2\left(\frac{H}{\rho}\right)^2 \left(\tilde{\theta} + \frac{4}{3}\tilde{\theta}^3 + \frac{17}{15}\tilde{\theta}^5 + \frac{248}{315}\tilde{\theta}^7\right). \quad (13)$$

This result is obtained as follows: The Taylor series of $f_{\tilde{\Theta}}(\tilde{\theta})$ can be represented as

$$f_{\tilde{\Theta}}(\tilde{\theta}) \approx f_{\tilde{\Theta}}(0) + \frac{f^{(1)}_{\tilde{\Theta}}(0)}{1!}\tilde{\theta} + \frac{f^{(2)}_{\tilde{\Theta}}(0)}{2!}\tilde{\theta} + \frac{f^{(3)}_{\tilde{\Theta}}(0)}{3!}\tilde{\theta} + \cdots, \quad (14)$$

where $f_{\tilde{\Theta}}(0) = 0$, $f^{(1)}_{\tilde{\Theta}}(0) = 2\,(H/\rho)^2$, $f^{(3)}_{\tilde{\Theta}}(0) = 8{\times}2\,(H/\rho)^2$, $f^{(5)}_{\tilde{\Theta}}(0) = 56 \times 2\,(H/\rho)^2$, $f^{(7)}_{\tilde{\Theta}}(0) = 3968 \times 2\,(H/\rho)^2$. In addition, $f^{(n)}_{\tilde{\Theta}}(0) = 0$ where n is an even number.

Therefore, it is true that the Taylor approximation of degree seven of $f_{\tilde{\Theta}}(\tilde{\theta})$ can be derived by substituting (14) as $2\,(H/\rho)^2\left(\tilde{\theta} + \frac{4}{3}\tilde{\theta}^3 + \frac{17}{15}\tilde{\theta}^5 + \frac{248}{315}\tilde{\theta}^7\right)$ that is equivalent to (13).

Thus, when the integrations of β_a and β_e are expressed in closed form, we can compute $E_{\tilde{\varphi},\tilde{\theta}}[\mathcal{I}^*]$ without numerical integration. The following results are based on this approximation for integration in the closed form.

Figs. 8 to 11 are the closed form approximation analysis results of $E_{\tilde{\varphi},\tilde{\theta}}[\mathcal{I}^*]$ with simulation results by changing parameters. Note that our simulation parameters are summarized in Table 1. The effect of pathloss on $E_{\tilde{\varphi},\tilde{\theta}}[\mathcal{I}^*]$ can be studied by Fig. 8. For better understanding of the results, we recall regions notations [A],[B], and [C] from Fig. 4. When pathloss is more severe (up to $n = 6$), region [A] is shrunk compared with the mild condition. When $n = -4$ or -6, region [A] is almost 0 m, and when $n = -2$, it is about 500 m. On the other hand, [B] and [C] are dependent upon pathloss. Note also that severe pathloss induces an overall drop in $E_{\tilde{\varphi},\tilde{\theta}}[\mathcal{I}^*]$.

The height of the FS receiver affects both regions of [A] and [B] as shown in Fig. 9. The higher FS receiver slightly moves the peak point of $E_{\tilde{\varphi},\tilde{\theta}}[\mathcal{I}^*]$ to the right side. In addition, region [B] and the mean interference power are also reduced by higher FS receiver. The effect of the height of the BSs on interference power is different than the effect of the height of the FS receiver. As shown in Fig. 10, the higher BSs slightly move the peak of $E_{\tilde{\varphi},\tilde{\theta}}[\mathcal{I}^*]$ to the left side. In addition, region [B] is increased by the higher FS receiver. However, the height of the BSs has a similar effect to the height of the FS receiver in terms of mean interference power. As shown in Fig. 11, the cell size ρ just changes the mean of $E_{\tilde{\varphi},\tilde{\theta}}[\mathcal{I}^*]$ without changing tendency.

V. CONCLUDING REMARKS

This paper conducted 28 GHz, 38 GHz, and 60 GHz mmWave frequency sharing impact research between cellular systems and fixed service (FS) systems in order to determine the necessary amount of frequency rejection, using both of numerical analysis and intensive simulations. In this frequency sharing study,

we calculated the amount of downlink and uplink interferences that were accumulated in an FS receiver antenna; and then we determined how much interference need to be suppressed in order to prevent harmful interference. This research is essential and mandatory prior to deploying mmWave cellular systems in order to verify whether the new systems will inject harmful interference into existing FS systems or not. If the newly deployed systems generate the interference, additional interference mitigation schemes need to be introduced. Therefore, this type of research is required before introducing new frequency bands in currently existing cellular networks. For this purpose, this paper verified how much interference should be suppressed based on numerical approximation and intensive simulations. For the numerical approximation, we derived closed-form results with Taylor series approximation. Finally, this paper confirmed that the numerical analysis results were precise, i.e., that here were only marginal differences to the intensive simulation results.

APPENDIX A
mmWave RADIO PROPAGATION

This appendix presents fundamental mmWave radio propagation characteristics, i.e., reference antenna radiation patterns [15], path-loss models, and attenuation factors.

For reference antenna radiation patterns [15], the ITU-recommended reference antenna patterns for sharing studies from 400 MHz to about 70 GHz are presented in [15]. As proposed in [15],

$$G(\varphi,\theta)=\begin{cases} G_{\max}-12|x|^2, & 0\le x<1,\\ G_{\max}-12-15\ln|x|, & 1\le x,\end{cases} \tag{15}$$

where $G_{\max}$ is a maximum antenna gain and $x \triangleq \Psi/\Psi_\alpha$ where

$$\Psi \triangleq \arccos\left(\cos\varphi\cos\theta\right), \tag{16}$$

$$\Psi_\alpha \triangleq \begin{cases} \frac{1}{\sqrt{\left(\frac{\cos\alpha}{\varphi_{\text{BW}}}\right)^2+\left(\frac{\sin\alpha}{\theta_{\text{BW}}}\right)^2}}, & 0^\circ\le\Psi\le 90^\circ,\\ \frac{1}{\sqrt{\left(\frac{\cos\theta}{\varphi_{3m}}\right)^2+\left(\frac{\sin\theta}{\theta_{\text{BW}}}\right)^2}}, & 90^\circ\le\Psi\le 180^\circ,\end{cases} \tag{17}$$

where φ and θ stand for azimuth and elevation angles ($-180^\circ \le \varphi \le 180^\circ$ and $-90^\circ \le \theta \le 90^\circ$); φ_{BW} and θ_{BW} stand for half-power beamwidth (HPBW) in the azimuth and elevation planes; and $\alpha = \arctan\left(\tan\theta/\sin\varphi\right)$, and φ_{3m} in (17) is the equivalent HPBW in the azimuth plane for an adjustment of horizontal gains (degrees), thus it can be calculated as $\varphi_{3m} = \varphi_{\text{BW}}$ for $0^\circ \le |\varphi| \le \varphi_{th}$ where φ_{th} is defined as the boundary azimuth angle (degrees), i.e., $\varphi_{th} = \varphi_{\text{BW}}$; and

$$\varphi_{3m}=\frac{1}{\sqrt{\left\{\frac{\cos\left(\frac{|\varphi|-\varphi_{th}}{180-\varphi_{th}}\times 90\right)}{\varphi_{\text{BW}}}\right\}^2+\left\{\frac{\sin\left(\frac{|\varphi|-\varphi_{th}}{180-\varphi_{th}}\times 90\right)}{\theta_{\text{BW}}}\right\}^2}} \tag{18}$$

for $\varphi_{th} < |\varphi| \le 180^\circ$.

The φ_{BW} and θ_{BW} can be calculated as follows [15] by assuming $\theta_{\text{BW}} \approx \varphi_{\text{BW}}$:

$$\theta_{\text{BW}} \approx \varphi_{\text{BW}} = \sqrt{31000\times 10^{-\frac{G_{\max}}{10}}}. \tag{19}$$

Table 2. Rain rates (unit: mm/h) and their corresponding attenuation factors (unit: dB/Km) at 28 GHz, 38 GHz, and 60 GHz bands [3].

f_c	ITU region	1% outage	0.1% outage
28 GHz	ITU region D (Northern CA, OR, WA)	2.1 mm/h (0.25 dB/Km)	8 mm/h (1.4 dB/Km)
	ITU region Q [Heavy rain] (Middle Africa, *et. al.*)	24 mm/h (4 dB/Km)	72 mm/h (12 dB/Km)
38 GHz	ITU region D (Northern CA, OR, WA)	2.1 mm/h (0.6 dB/Km)	8 mm/h (2.0 dB/Km)
	ITU region Q [Heavy rain] (Middle Africa, *et. al.*)	24 mm/h (6 dB/Km)	72 mm/h (17 dB/Km)
60 GHz	ITU region D (Northern CA, OR, WA)	2.1 mm/h (1.2 dB/Km)	8 mm/h (3.5 dB/Km)
	ITU region Q [Heavy rain] (Middle Africa, *et. al.*)	24 mm/h (9 dB/Km)	72 mm/h (25 dB/Km)

For path-loss models, free-space basic transmission loss in a dB scale is given as a function of path length d_{Km} in a Km scale [16]:

$$PL\left(f_c, d_{\text{Km}}\right) = 92.44 + 20\log_{10}\left(f_c\right) - n\times 10\log_{10}\left(d_{\text{Km}}\right), \tag{20}$$

where f_c stands for the carrier frequencies in a GHz scale and n is path-loss coefficient that is set to $-2.2 \le n \le -1.9$ for line-of-sight (LoS) propagation when $f_c \ge 10$ [16] (note that we consider $n = -2.2$ in this paper, as a representative). Even though non-line-of-sight (NLoS) propagation is also of interest, mmWave NLoS path-loss models for long-distance scenarios (from 1 Km to 50 Km) has not been investigated yet, to the best of our knowledge. In addition, ITU-R P.1411 [16] clearly states that mmWave signal coverage is considered only for free-space propagation because of the large diffraction losses experienced when obstacles cause the propagation path to become NLoS.

For mmWave specific attenuation factors, attenuation by atmospheric gases (i.e., oxygen attenuation) and by rain must be considered in mmWave propagation [16]. The oxygen attenuation behaviors depending on carrier frequencies are obtained from [17] and the oxygen attenuation factors in 28 GHz, 38 GHz, and 60 GHz mmWave bands are 0.11 dB/Km, 0.13 dB/Km, and 16 dB/Km, respectively. The rain attenuation factors depend on the rain climatic zones, and those are segmented and measured by the ITU as presented in ITU recommendation ITU-R PN.837-1 [18]. Table 2 in [18] presents rain rates depending on the segmented areas (from ITU region A to ITU region Q). In this paper, ITU region D (Northern California (CA), Oregon (OR), and Washington (WA)) and ITU region Q (the heaviest rain areas such as Middle Africa) are of interest. Table 2 presents the rain rates of ITU regions D and Q (unit: mm/h); and their corresponding rate attenuation factors (unit: dB/Km) depending on various outage probabilities (1.0% and 0.1%) based on [19]. Table 2 presents rain attenuation factors in (i) various ITU regions D and Q, various outage probabilities (1.0% and 0.1%), and (iii) various mmWave bands, i.e., 28 GHz, 38 GHz, and 60 GHz.

REFERENCES

[1] J. Kim, L. Xian, R. Arefi, A. Maltsev, and A. S. Sadri, "Study of coexistence between 5G small-cell systems and systems of the fixed service at 39 GHz band," in *Proc. IEEE MTT-S IMS*, May 2015.

[2] J. Kim, L. Xian, R. Arefi, and A. S. Sadri, "60 GHz frequency sharing study

between fixed service systems and small-cell systems with modular antenna arrays," in *Proc. IEEE GLOBECOM Wkshps*, Dec. 2015.

[3] J. Kim, L. Xian, and A. S. Sadri, "Numerical simulation study for frequency sharing between micro-cellular systems and fixed service systems in millimeter-wave bands," *IEEE Access*, vol. 4, pp. 9847–9859, Dec. 2016.

[4] M. Baianifar, S.M. Razavizadeh, H. Akhlaghpasand, and I. Lee, "Energy efficiency maximization in mmWave wireless networks with 3D beamforming," *J. Commun. Netw.*, vol. 21, no. 2, pp. 125–135, Apr. 2019.

[5] A. Hu, "Channel estimation for interference mitigation in millimeter-wave multi-Cell beamspace MIMO systems," *J. Commun. Netw.*, vol. 19, no. 4, pp. 371–383, Aug. 2017.

[6] J.-S. Sheu, "Hybrid digital and analogue beamforming design for millimeter wave relaying systems," *J. Commun. Netw.*, vol. 19, no. 5, pp. 461–469, Oct. 2017.

[7] W. Roh, *et al.*, "Millimeter-wave beamforming as an enabling technology for 5G cellular communications: Theoretical feasibility and prototype results," *IEEE Commun. Mag.*, vol. 52, no. 2, pp. 106–113, Feb. 2014.

[8] W. Hong, K. H. Baek, Y. Lee, Y. Kim, and S. T. Ko, "Study and prototyping of practically large-scale mmWave antenna systems for 5G cellular devices," *IEEE Commun. Mag.*, vol. 52, no. 9, pp. 63–69, Sept. 2014.

[9] T. Rappaport, F. Gutierrez, E. Ben-Dor, J. Murdock, Y. Qiao, and J. Tamir, "Broadband millimeter-wave propagation measurements and models using adaptive-beam antennas for outdoor urban cellular communications," *IEEE Trans. Antennas Propagation*, vol. 61, no. 4, pp. 1850–1859, Apr. 2013.

[10] T. Rappaport, J. Murdock, and F. Gutierrez, "State of the art in 60-GHz integrated circuits and systems for wireless communications," *Proc. IEEE*, vol. 99, no. 8, pp. 1390–1436, Aug. 2011.

[11] *System parameters and considerations in the development of criteria for sharing or compatibility between digital fixed wireless systems in the fixed service and systems in other services and other sources of interference*, ITU-R F.758-5, Mar. 2012.

[12] *Evolved universal terrestrial radio access (E-UTRA); radio frequency (RF) system scenarios*, *3GPP 36.942*, 2012.

[13] *Possibility of sharing between fixed links and SNG in the 14.25 - 14.5 GHz Band*, ERC Report 39, Oct. 1996.

[14] A. Maltsev, *et al.*, *Millimetre-wave evolution for backhaul and access (MiWEBA) WP5 D5.1: Channel modeling and characterization*, MiWEBA Project Document, EU Contract No. FP7-ICT-608637, 2014.

[15] *Reference radiation patterns of omnidirectional, sectoral and other antennas for the fixed and mobile services for use in sharing studies in the frequency range from 400 MHz to about 70 GHz*, ITU-R F.1336-4, Feb. 2014.

[16] *Propagation data and prediction methods for the planning of short-range outdoor radiocommunication systems and radio local area networks in the frequency range 300 MHz to 100 GHz*, ITU-R P.1411-8, July 2015.

[17] *Attenuation by atmospheric gases*, ITU-R P.676-10, Sept. 2013.

[18] *Characteristics of precipitation for propagation modelling*, ITUR PN.837-1, 1994.

[19] *Federal communications commission (FCC), office of engineering and technology*, Bulletin Number 70, July 1997.

Sungmin Han received his B.S. degree in Electronics Engineering from Korea University of Technology and Education, Cheonan, South Korea, in 2012, and his Ph.D. degree in Information and Communicaiton Engineering from Daegu Gyeongbuk Institute of Science and Technology (DGIST), Daegu, South Korea, in 2019, respectively. Since 2019, he has been a communication system designer with VSI, Seoul, South Korea. His current research interests include communication theory and automotive communication IC design such as in-vehicle SerDes and Ethernet.

Ji-Woong Choi received the B.S., M.S., and Ph.D. degrees from Seoul National University (SNU), Seoul, South, Korea, in 1998, 2000, and 2004, respectively, all in Electrical Engineering. From 2004 to 2005, he was a Postdoctoral Researcher with the Inter University Semiconductor Research Center, SNU. From 2005 to 2007, he was a Postdoctoral Visiting Scholar with the Department of Electrical Engineering, Stanford University, Stanford, CA, USA. He was also a Consultant for GCT Semiconductor, San Jose, CA, USA, for development of mobile TV receivers from 2006 to 2007. From 2007 to 2010, he was with Marvell Semiconductor, Santa Clara, CA, USA, as a Staff Systems Engineer for next-generation wireless communication systems, including WiMAX and LTE. Since 2010, he has been with the Information and Communication Engineering Department, Daegu Gyeongbuk Institute of Science and Technology (DGIST), Daegu, South Korea, as a Full Professor, and also working as Director of Brain Engineering Convergence Research Center, DGIST. His research interests include communication theory and signal processing, and related applications such as vehicular communications, biomedical signal processing/machine learning applications, brain–machine/computer interface (BMI/BCI), and near-field wireless power transfer. He is Editor of Journal of Communications and Networks (JCN) and IEEE Transactions on Molecular, Biological, and Multi-Scale Communications (TMBMC).

Joongheon Kim is currently an Assistant Professor of Electrical Engineering with Korea University, Seoul, Korea, since 2019. He received his B.S. (2004) and M.S. (2006) in Computer Science and Engineering from Korea University, Seoul, Korea; and his Ph.D. (2014) in Computer Science from the University of Southern California (USC), Los Angeles, CA, USA. Before joining Korea University as an Assistant Professor, he was with LG Electronics as a Research Engineer (Seoul, Korea, 2006–2009), InterDigital as an Intern (San Diego, CA, USA, 2012), Intel Corporation as a Systems Engineer (Santa Clara, CA, USA, 2013–2016), and Chung-Ang University as an Assistant Professor of Computer Science and Engineering (Seoul, Korea, 2016–2019). He is a Senior Member of the IEEE. He was a recipient of the Annenberg Graduate Fellowship with his Ph.D. admission from USC (2009) and the Haedong Young Scholar Award (2018) which is for recognizing a young Korean researcher under the age of 40 who has made outstanding scholarly contributions to communications and information sciences research.

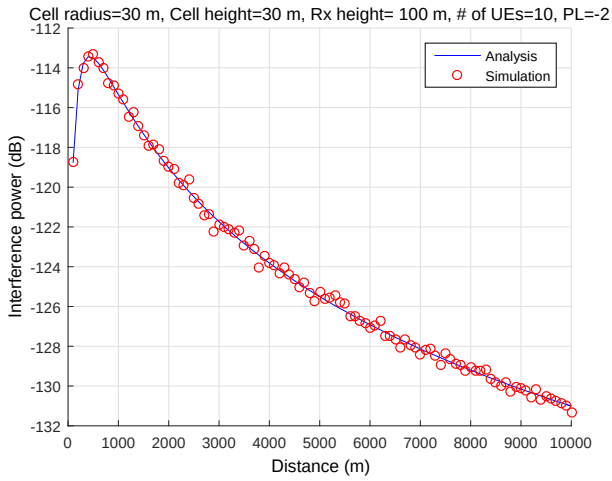

(a)

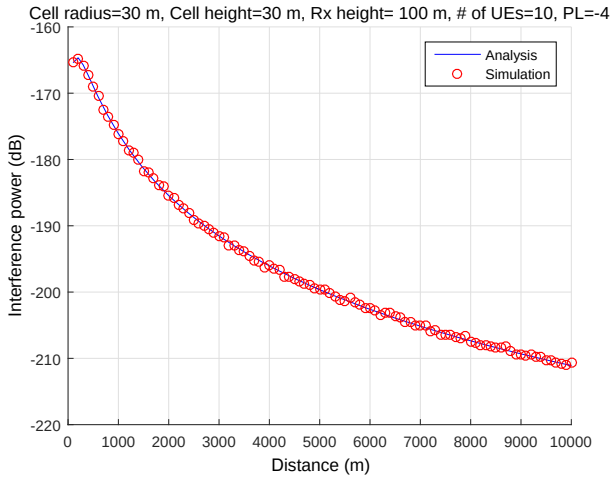

(b)

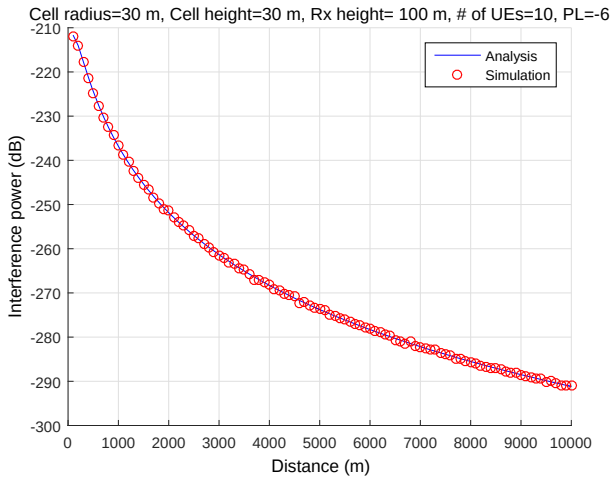

(c)

Fig. 8. Interference power with varying pathloss: (a) $n = -2$, (b) $n = -4$, and (c) $n = -6$.

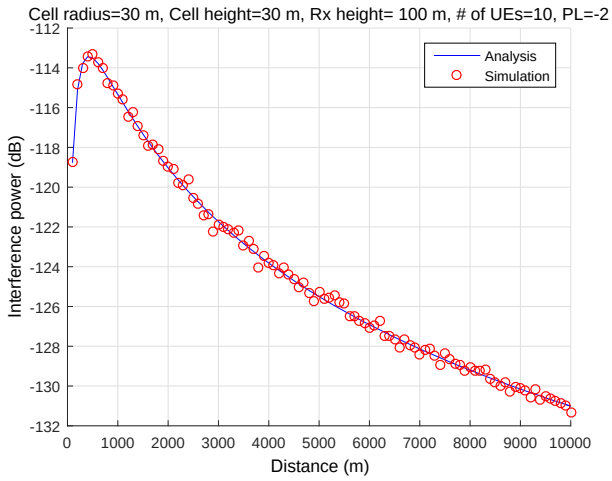

(a)

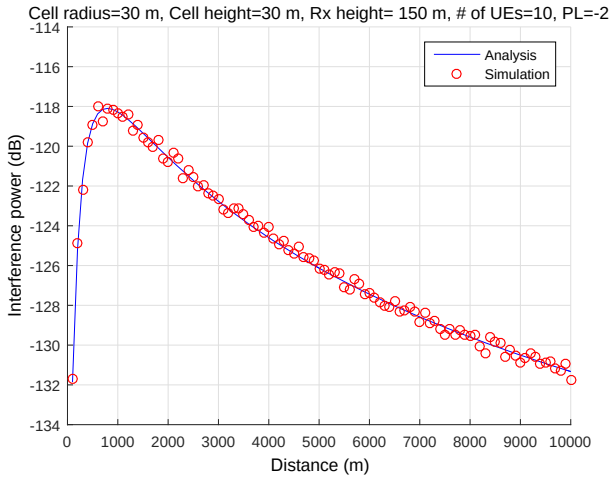

(b)

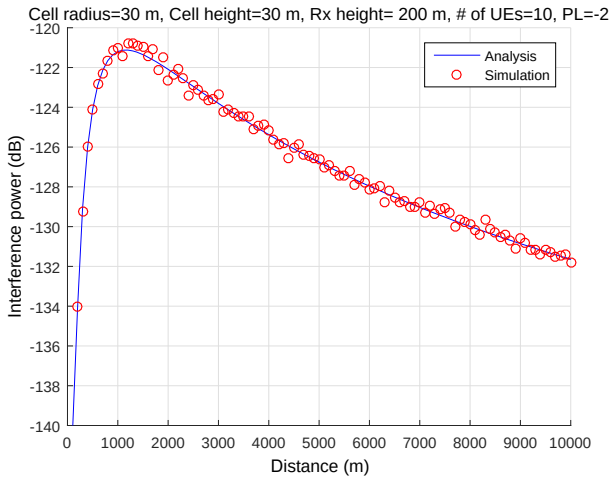

(c)

Fig. 9. Interference power with varying height of FS receiver: (a) FS height= 100 m, (b) FS height= 150 m, and (c) FS height= 200 m.

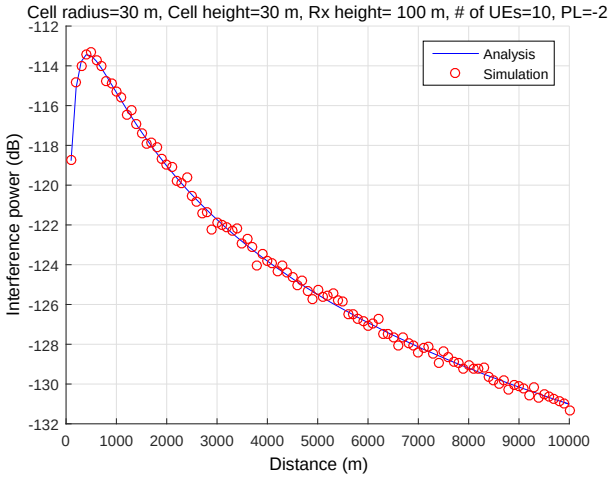

(a)

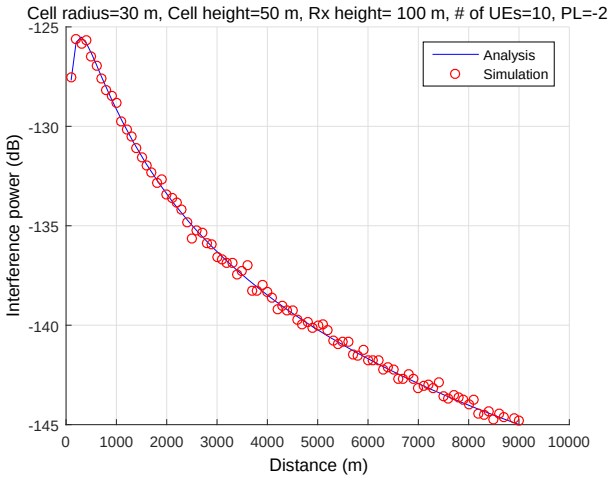

(b)

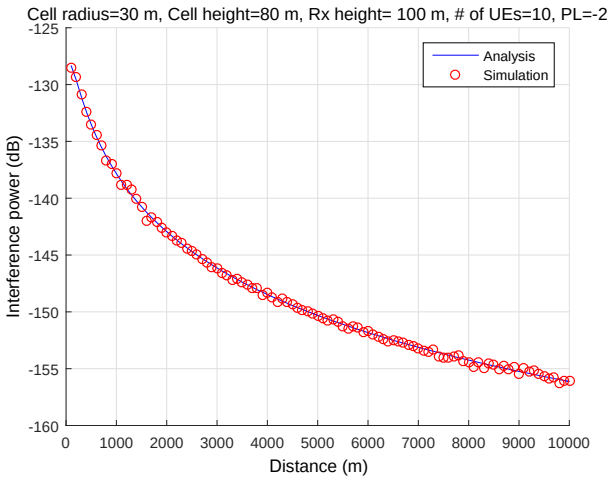

(c)

Fig. 10. Interference power with varying height of BSs: (a) BSs height$= 30\,m$, (b) BSs height$= 50\,m$, and (c) BSs height$= 80\,m$.

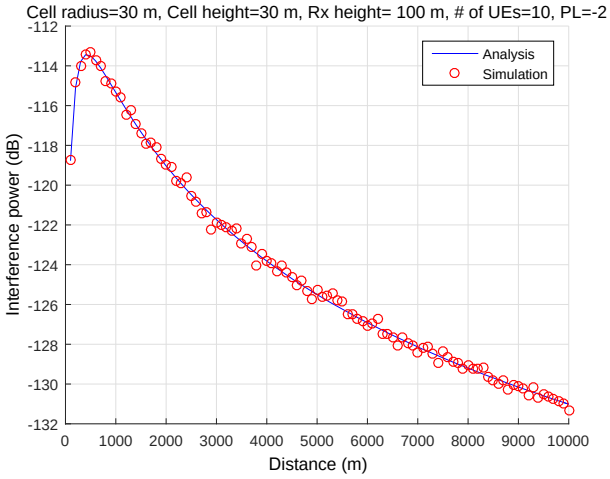

(a)

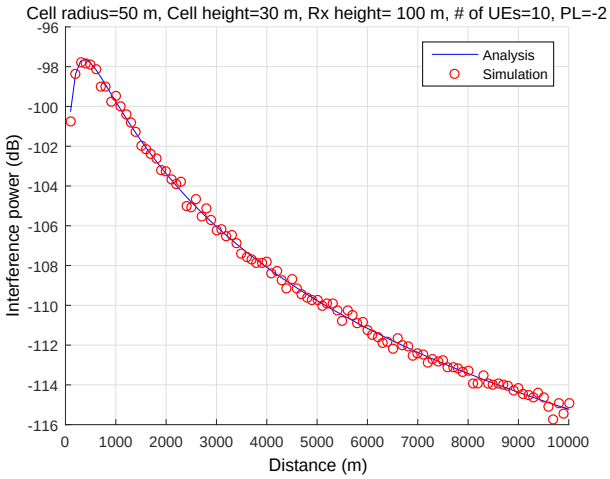

(b)

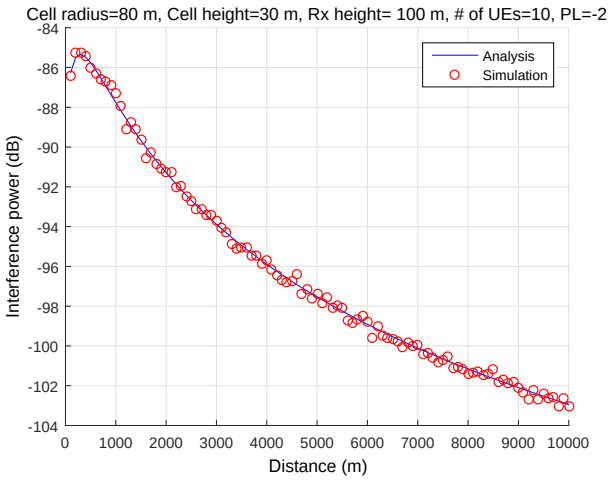

(c)

Fig. 11. Interference power with varying ρ: (a) $\rho = 30\,m$, (b) $\rho = 50\,m$, and (c) $\rho = 80\,m$.